Detrital zircon U–Pb geochronology of the upper Carboniferous strata of Hala'alat Mountain, West Junggar: implications for provenance

Xingyu Chen[1] , Zhijie Zhang[2], Xuanjun Yuan[2], Yinhe Liu[2], Dawei Cheng[2], Li Wan[2] and Chuanmin Zhou[2]

[1]School of Earth and Space Sciences, Peking University, Beijing 100871, China and [2]Research Institute of Petroleum Exploration and Development, PetroChina, Beijing 100083, China

Abstract

During late Carboniferous time, the residual ocean basin gradually closed in West Junggar and only a small amount of seawater remained in the Hala'alat Mountain area, where discussions of provenance and tectonics are limited. In this study, LA-ICP-MS U–Pb dating and heavy mineral identification are conducted on the upper Carboniferous tuffaceous sandstones from the Hala'alat and Aladeyikesai formations in the Hala'alat Mountain area. The results reveal the low maturity of the clastic sediments, indicating proximal deposition. The Hala'alat Formation detrital zircons present a single peak (*c.* 330 Ma). Speculatively, the primary provenance is the Boshchekul–Chingiz Arc, and the secondary sources are the Darbut Tectono-Magmatic Belt and island arcs in the basin. The main peak and provenance of the Aladeyikesai Formation are similar to those of the Hala'alat Formation. Moreover, several age groups, namely, 370–344 Ma, 427–404 Ma and 478–476 Ma, potentially correspond to provenances of the Darbut Tectono-Magmatic Belt, the Boshchekul–Chingiz Arc and the Kujibai–Hongguleleng Ophiolitic Mélange Belt. In addition, the maximum depositional ages of the Hala'alat and Aladeyikesai formations calculated are 314.6 ± 1.54 Ma and 330.8 ± 0.61 Ma, respectively. Comprehensive analysis shows a relatively singular provenance of the Hala'alat Formation. While the provenance of the Aladeyikesai Formation shows inheritance, the provenance area extends northwards to the Kujibai–Hongguleleng Ophiolitic Mélange Belt. Furthermore, the closure of the Junggar Ocean during Carboniferous time caused the potential source region of the Hala'alat Mountain area to migrate northeastwards from Barleik Mountain to Xiemisitai Mountain. This study provides a basis for the analysis of regional geological evolution.

1. Introduction

West Junggar is located in the southern Central Asian Orogenic Belt and has a complex tectonic background and rich mineral resources. Hala'alat Mountain (HLM) is located on the NW margin of the Junggar Basin and is an extension of Zaire Mountain (ZRM) in the NE direction. The Mahu Sag in the south is an important oil exploration area (Xiao *et al.* 2008; Zhang *et al.* 2011; Choulet *et al.* 2012b) (Fig. 1). Geochronology and provenance analysis of the upper Carboniferous strata in the HLM area is helpful for understanding the sedimentary system, the distribution and characteristics of source rocks, and the evolutionary role of tectonics and palaeogeography in the Junggar Basin.

At present, research on Carboniferous strata in West Junggar mainly focuses on stratigraphic correlation and tectonic evolution (Jian *et al.* 2005; Geng *et al.* 2011; Yang *et al.* 2016; Yin *et al.* 2017); this research provides references for provenance analysis of the HLM area in West Junggar in terms of the tectonic background, palaeogeographic pattern, etc. However, few studies have reported on the provenance of the upper Carboniferous sedimentary rocks in the HLM area. Previous research on the upper Carboniferous strata in the HLM area has mainly determined the stratigraphic ages, reconstructed the sedimentary environment (Tao *et al.* 2017; Ma, 2018) and tectonic background (Zong *et al.* 2014; Gong & Zong, 2015; Xiang, 2015) through palaeontological analysis (Wei, 1983; Wang *et al.*, 1987), dated effusive rocks (Xiang *et al.* 2013a,b; Li, G. Y. *et al.* 2016) and conducted geochemical and other analyses. Only Tao *et al.* (2013) studied the provenances of the sedimentary rocks of the Hala'alat Formation in the HLM area through geochemistry; their findings suggested that the main provenance is the Saur magmatic arc and that the secondary provenances are the Boshchekul–Chingiz Arc (BCA) and the oceanic arc in the Kexia area.
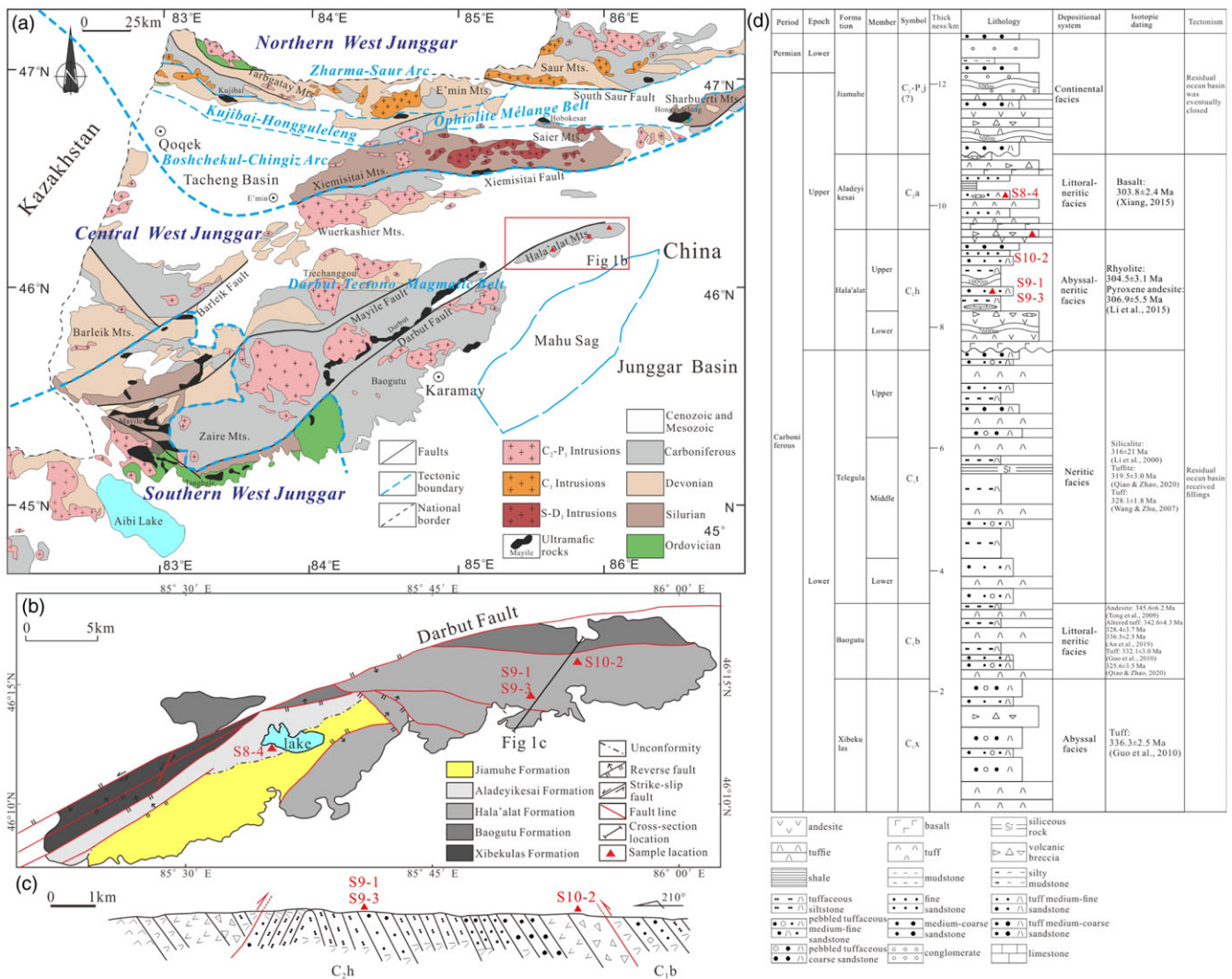
Fig. 1. (Colour online) (a) Simplified geological map of West Junggar (modified after Yang, 2012). The red triangles are the locations of the sampling points. The red box shows the location of the study area. (b) Regional geological sketch of Hala'alat Mountain in West Junggar. Modified after a new 1:50 000 geological survey report from the China Geological Survey (Li, G. Y. et al. 2016). (c) Simplified cross-section and (d) simplified stratigraphic column of Hala'alat Mountain, West Junggar.

This research studies the sandstones of the upper Carboniferous Hala'alat and Aladeyikesai formations in the HLM area. Through detrital zircon U–Pb geochronology, petrographic characteristics and heavy mineral analysis, this paper comprehensively analyses the source of the upper Carboniferous clastic rocks in the HLM area and investigates potential provenances, which are combined with the surrounding stratigraphic distribution observations, igneous zircon geochronology data and regional tectonic characteristics. This paper provides a scientific basis for studying the characteristics of source-to-sink systems and tectonic evolution.

2. Overview of regional geology

West Junggar is mainly composed of the Zharma–Saur Arc (ZhSA), the Kujibai–Hongguleleng Ophiolitic Mélange Belt (KHOMB) and the BCA in the north, an accretionary complex in the central area and a magmatic arc in the south (Fig. 1) (Windley et al. 2007; Zhang et al. 2011; Liu et al. 2017). Moreover, the Darbut Tectono-Magmatic Belt (DTMB) in central

West Junggar consists of the Darbut Ophiolitic Mélange, ZRM and HLM.

During the Devonian Period, the Junggar Ocean in the central and northern West Junggar area widely subducted and collaged to form an archipelago arc-basin system. With the subsequent evolution of the residual Junggar Ocean (Yang et al. 2015), the scale of the ocean basin gradually decreased along with its closure. West Junggar experienced two different stages of tectonic evolution, namely, a fore-arc basin in early Carboniferous time and a residual sea in late Carboniferous time (Xiang, 2015). During early Carboniferous time, the HLM–ZRM area began to receive large-scale inputs of peripheral pyroclastic materials (Gao et al. 2013), and the Xibekulas Formation, Baogutu Formation and Telegula Formation were successively deposited, forming a set of continuous and thick marine terrigenous clastic rocks. The detrital sediments came from the effusive rocks of the island fore-arc type that formed in the same period (Guo et al. 2010; Geng et al. 2011; Xiang, 2015). In late Carboniferous time, regional large-scale regression occurred, and only a small amount of seawater remained in the HLM area (Zong et al. 2014). A set of

volcanic-terrigenous clastic strata of bathyal to littoral-neritic facies was deposited: during the sedimentary period of the Hala'alat Formation, magmatic activity was intense and the content of volcanic clasts in the sediments was high (Li, G. Y. *et al.* 2016); the resulting Aladeyikesai Formation is dominated by terrigenous clastic rocks in littoral-neritic facies and is the uppermost layer of preserved marine sediments in the HLM area (Peng *et al.* 2016). By the end of late Carboniferous time, all the seawater in the HLM area had retreated, and a large-scale intracontinental orogeny began. A set of molasse formations in alluvial fan – fan delta facies represented by the Jiamuhe Formation was deposited above the Aladeyikesai Formation in angular unconformity (Table 1), indicating that the residual ocean basin in West Junggar finally closed during the end of the late Carboniferous period (Gong & Zong, 2015; Zhang, 2020).

3. Sample collection and petrological characteristics

In this study, tuffaceous sandstone samples of the upper Carboniferous Hala'alat and Aladeyikesai formations were collected in the HLM area. The sampling locations and layers are shown in Figure 1. Contact, alteration and fractured zones were avoided as much as possible to ensure that the samples were weakly altered, relatively fresh and representative.

3.a. Sedimentary and microscopic characteristics

3.a.1. Hala'alat Formation
The samples collected from the Hala'alat Formation in this study are tuffaceous fine- to medium-grained feldspar lithic sandstone, with sample numbers of S9-1 and S9-3, and the sampling location is 85° 51′ 7″ E, 46° 14′ 35″ N. The field section shows clear stratigraphic bedding, and the sedimentary cycles include volcanic breccia and tuffaceous sandstone from bottom to top (Fig. 2a, b).

The hand specimens are grey and massive in structure. The detritus mainly consists of debris (65 %), feldspar (22 %), quartz (3 %) and interstitial materials (10 %), with grain sizes ranging from 0.1 to 1 mm and occasional gravel grains. Most of the debris grains are angular and subangular, with poor sorting, high contents of debris and feldspar, and low overall textural and compositional maturity, indicating that the debris grains have not been transported for a long distance and are relatively proximal products. Among these grains, the feldspars are intermediate-basic plagioclase with twinned crystal characteristics and wider twinned crystal seams. Some of the grain surfaces are degraded owing to alteration. The quartz surfaces are cleaner and lack alteration. The interstitial fillings are mainly tuff. The lithic fragments are mainly tuff debris and andesite debris, minor gabbro-diabase debris and occasional acidic effusive rock or siliceous rock debris (Fig. 2c, d). The sandstone petrology indicates that the provenance is adjacent intermediate-basic igneous rocks.

3.a.2. Aladeyikesai Formation
The samples collected in this study are fine-grained tuffaceous feldspar lithic sandstones, with sample numbers S8-4 and a sampling location of 85° 35′ 11″ E, 46° 12′ 23″ N. Field observations indicate that the rocks are grey overall with clear and graded bedding. Tuffaceous sandstone and volcanic breccia are interbedded (Fig. 3a–c).

According to microscopic observations, the samples are composed of debris (65–70 %), feldspar (15–20 %), quartz (10 %) and interstitial materials (5 %), with grain sizes ranging from 0.1

to 0.25 mm. Among these components, feldspars are generally altered, contain multiple twins and are mainly plagioclases and occasionally alkaline feldspars. Their petrographic characteristics are similar to those of the aforementioned Hala'alat Formation sandstone (Fig. 3d, e), indicating that the sediments are mainly from nearby igneous rocks, but the tuff content is lower than that of the Hala'alat Formation sandstone.

3.b. Assemblage and characteristics of heavy minerals

Heavy mineral identification and analysis was carried out on the aforementioned sandstone samples and pyroclastic samples of the Hala'alat Formation (sample number: S10-2; sampling point location: 85° 53′ 52″ E, 46° 15′ 57″ N). The above procedures were completed by Chengxin Geological Services Co., Ltd, Langfang, Hebei Province.

The results show that the contents of all types of iron ores in the samples are generally higher (Table 2). The heavy mineral assemblage of the Hala'alat Formation sandstone is magnetite–epidote–ilmenite–hornblende. The heavy minerals in the pyroclastic sandstone are mainly pyroxene and minor serpentine, which is a special light mineral, and the heavy minerals have a relatively high unstable mineral content and low maturity. The Aladeyikesai Formation sandstone mainly has a heavy mineral assemblage of leucoxene–Cr-spinel–apatite dominated by stable heavy minerals.

4. Test method and data processing

Zircon separation, selection, sample target preparation and photography were completed by Chengxin Geological Services Co., Ltd, Langfang, Hebei Province. Cathodoluminescence (CL) images were taken by a scanning electron microscope (Gatan MonoCL3+ X). The selected zircon grains have smooth surfaces and are transparent under transmitted light, reflected light and CL imaging. The spots for dating were selected in the areas without cracks and inclusions, but no bias in the shapes and sizes of detrital zircons was present.

Zircon U, Th and Pb isotope data were obtained by laser ablation inductively coupled plasma mass spectrometry (LA-ICP-MS) at the State Key Laboratory of Continental Dynamics, Northwestern University. A detailed description of the method is presented in the Appendix.

Data processing was carried out by ICPMSDataCal 11.8 software, common lead correction was conducted by software developed by Andersen (2002) and age calculations and harmonic plot drawings were completed by ISOPLOT 2.49. The age probability density map was drawn using detritalPy software (Sharman *et al.* 2018) by selecting zircon concordance degrees between 90 % and 100 %, and the maximum sedimentary age was calculated.

5. Analysis results

5.a. Zircon characteristics and genesis

The zircon U–Pb geochronology of the upper Carboniferous tuffaceous sandstones (samples S9-3 from the Hala'alat Formation and S8-4 from the Aladeyikesai Formation) in the HLM area was analysed, and the results are shown in online Supplementary Material Tables S1 and S2, respectively.

Under the microscope, the zircons tested in this study generally have the following characteristics: most of them have complete crystal shapes, high automorphic degrees and granular or short columnar shapes, while a few have long columnar and elliptical

Table 1. Characteristics of the Carboniferous strata of Hala'alat Mountain, West Junggar

System	Series	Formation	Index	Contact relationship with overlying strata	Lithologic feature	Depositional system	Stratigraphic deposit age	Tectonism
Permian	Lower	Jiamuhe	C_2-P_1j (?)	Angular disconformity	The lower part is composed of intermediate-acidic continental effusive rocks and pyroclastic rocks. The upper part is a molasse formation.	Continental facies		Residual ocean basin eventually closed
Carboniferous	Upper	Aladeyikesai	C_2a	Angular disconformity	Mainly clastic and calcareous clastic rocks with more biolithite lenses.	Littoral-neritic facies	Basalt: 303.8 ± 2.4 Ma (Xiang, 2015)	Residual ocean basin received sediment
		Hala'alat	C_2h	Conformity	The lower part is mainly effusive rocks and pyroclastic rocks and contains more limestone lenses. The upper part is mainly powder fine-grained turbidites, and the content of coarse terrigenous clastic sediments increases gradually upwards, with few bioclastic limestone bands.	Abyssal-neritic facies	Rhyolite: 304.5 ± 3.1 Ma Pyroxene andesite: 306.9 ± 5.5 Ma (Li, G. Y. *et al.* 2015)	
	Lower	Telegula	C_1t	Angular disconformity	The pyroclastic rocks are coarser in the lower part and finer in the upper part, with high siliceous content in the upper part intercalated with siliceous rocks and fewer intermediate-basic volcanic rocks.	Neritic facies	Silicalite: 316 ± 21 Ma (Li *et al.* 2000) Tuffite: 319.5 ± 3.0 Ma (Qiao & Zhao, 2020) Tuff: 328.1 ± 1.8 Ma (Wang & Zhu, 2007)	
		Baogutu	C_1b	Conformity	Fine-grained pyroclastic rocks with good stratification and well-developed bedding partially intercalated with fewer coarser-grained pyroclastic rocks and limy lenses.	Littoral-neritic facies	Andesite: 345.6 ± 6.2 Ma (Tong *et al.* 2009) Altered tuff: 342.6 ± 4.3 Ma, 328.4 ± 3.7 Ma, 336.5 ± 2.5 Ma (An *et al.* 2019) Tuff: 332.1 ± 3.0 Ma (Guo *et al.* 2010), 325.6 ± 3.5 Ma (Qiao & Zhao, 2020)	
		Xibekulas	C_1x	Conformity	Coarser-grained pyroclastic rocks with poor stratification and undeveloped bedding intercalated with fewer fine-grained pyroclastic rocks, with synsedimentary biological limestone blocks.	Abyssal facies	Tuff: 336.3 ± 2.5 Ma (Guo *et al.* 2010)	

The relatively new and old sequence and ages of the Xibekulas, Baogutu and Telegula formations are controversial. Some scholars believe that the Jiamuhe Formation was deposited in late Carboniferous time (Zong *et al.* 2014).

granular shapes. The zircon surfaces are slightly rough, with black inclusions. Few zircon cracks and edges are corroded. The long/short ratios of the zircon grains are 1.2–3.0, and most are within 1.5–2.0, and the grain diameters are 50–200 μm. The grain diameters of the detrital zircons from the Hala'alat Formation are mainly in the range of 50–120 μm, while those from the Aladeyikesai Formation are in the range of 60–150 μm. Most detrital zircons are poorly rounded and angular to subangular, with no obvious transport traces.

Th/U ratios are related to zircon genesis (Belousova *et al.* 2002): magmatic zircons have a higher Th/U ratio (>0.4), while metamorphic zircons have a lower Th/U ratio (<0.1). In the two samples in this study, almost all zircons have clear oscillating zones (Figs 4a, 5a), and fan-shaped zoning occurs in a few zircon grains.
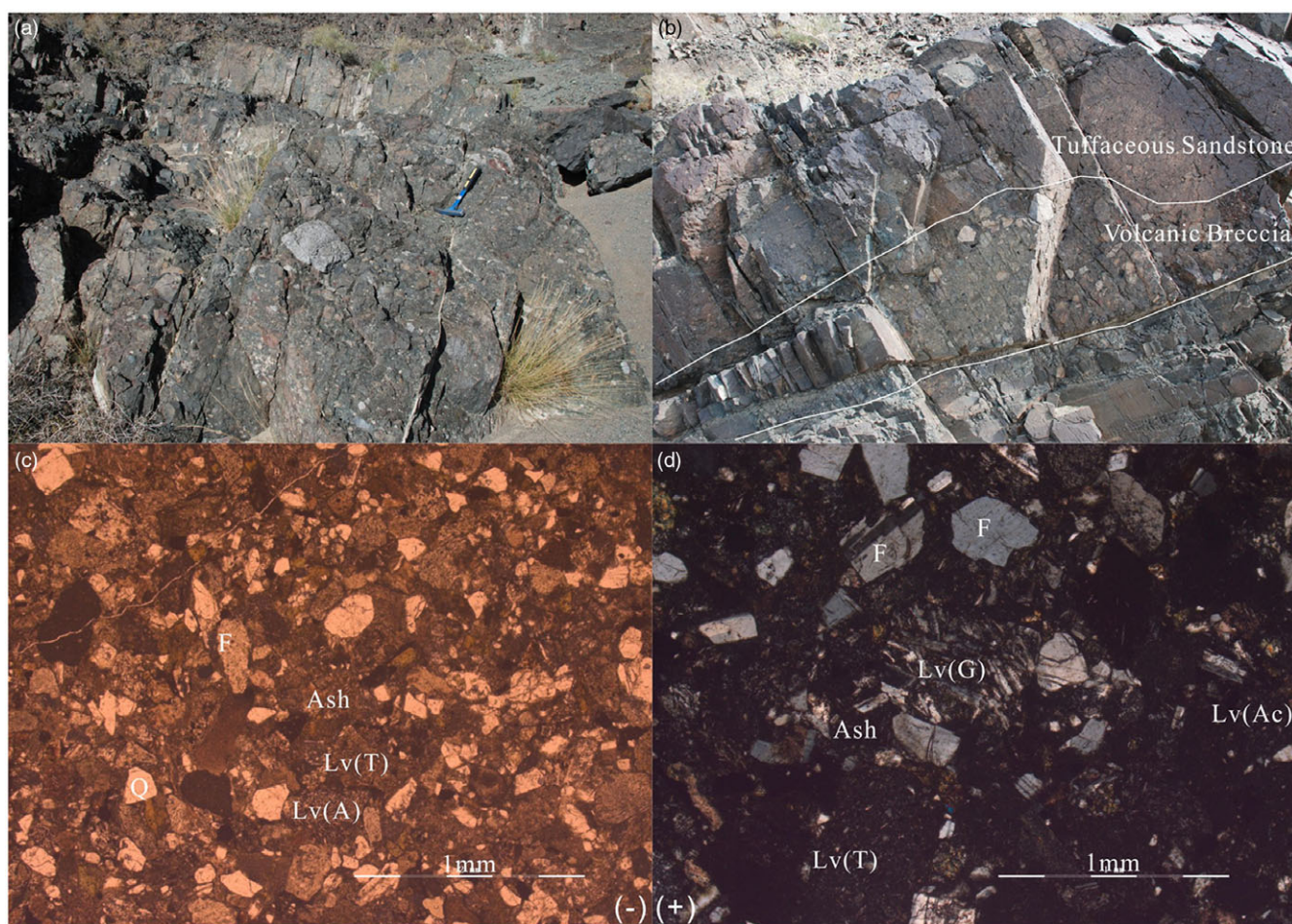
Fig. 2. (Colour online) (a, b) Field photographs of the Hala'alat Formation on Hala'alat Mountain. (c, d) Photomicrographs of selected sandstone samples under (c) plane-polarized and (d) cross-polarized light. Abbreviations of minerals: A – andesite; Ac – acidic effusive rock; Ash – volcanic ash; F – feldspar; G – gabbro; Lv – volcanic lithic fragment; Q – quartz; T – tuff.

Approximately 80 % of the zircon grains have Th/U ratios greater than 0.4 (see online Supplementary Material Tables S1 and S2), indicating that the zircons are of magmatic origin.

5.b. Detrital zircon U–Pb ages

From the 96 tested zircon grains in sandstone samples from the Hala'alat Formation, the U–Pb concordance degrees of 84 zircon grains range from 90 % to 100 % (Fig. 4c). The ages of most zircons are 340–320 Ma (Fig. 4d). An obvious peak occurs at 330 Ma and accounts for 74 % of the total, indicating that the provenance is relatively simple and is mainly from early Carboniferous igneous rocks. In addition, 9 % of zircon grains are Devonian, 9 % are late Carboniferous and a few are Ordovician and Silurian (Fig. 4b).

A total of 100 age measurement points were analysed for the sandstone samples from the Aladeyikesai Formation. Among these points, 88 zircons have a high concordance degree, almost all of which plot on the concordia line. Only a few grains plot below the concordia line, which may be caused by Pb loss due to hydrothermal activity (Fig. 5c). Zircon grains range in age from 319.9 ± 3.5 Ma to 484.9 ± 5.3 Ma, with most of the data concentrated within 320–380 Ma. Sixty-six per cent of the zircons are early Carboniferous, 23 % are Devonian and 11 % are late Palaeozoic (Fig. 5b). The age distribution curve shows a multipeak

form, with a primary peak age of 331 Ma (Fig. 5d) and secondary peak ages of 343 Ma, 365 Ma, 405 Ma, 424 Ma and 477 Ma, indicating a relatively complex provenance.

In conclusion, the ages of zircons in the Hala'alat and Aladeyikesai formations are concentrated in the range of 335–325 Ma, and the main peak ages are similar, indicating that the zircons may have the same provenance. However, several secondary peaks are present in the Aladeyikesai Formation, suggesting that the source of the Aladeyikesai Formation may be more complex than that of the Hala'alat Formation.

6. Discussion

6.a. Maximum depositional age (MDA)

The youngest detrital zircon age is one of the commonly used methods to estimate the maximum depositional age (MDA) (Sharman *et al.* 2018). The youngest single grain (YSG) data will indicate a younger age than the true age of deposition, mainly owing to Pb loss, and the inherent lack of reproducibility diminishes confidence in the reliability of this approach (Gehrels, 2014). From a statistical point of view, the youngest-age measures based on multiple grain ages provide solutions to this bias towards younger ages, and multiple grain ages are more consistently compatible
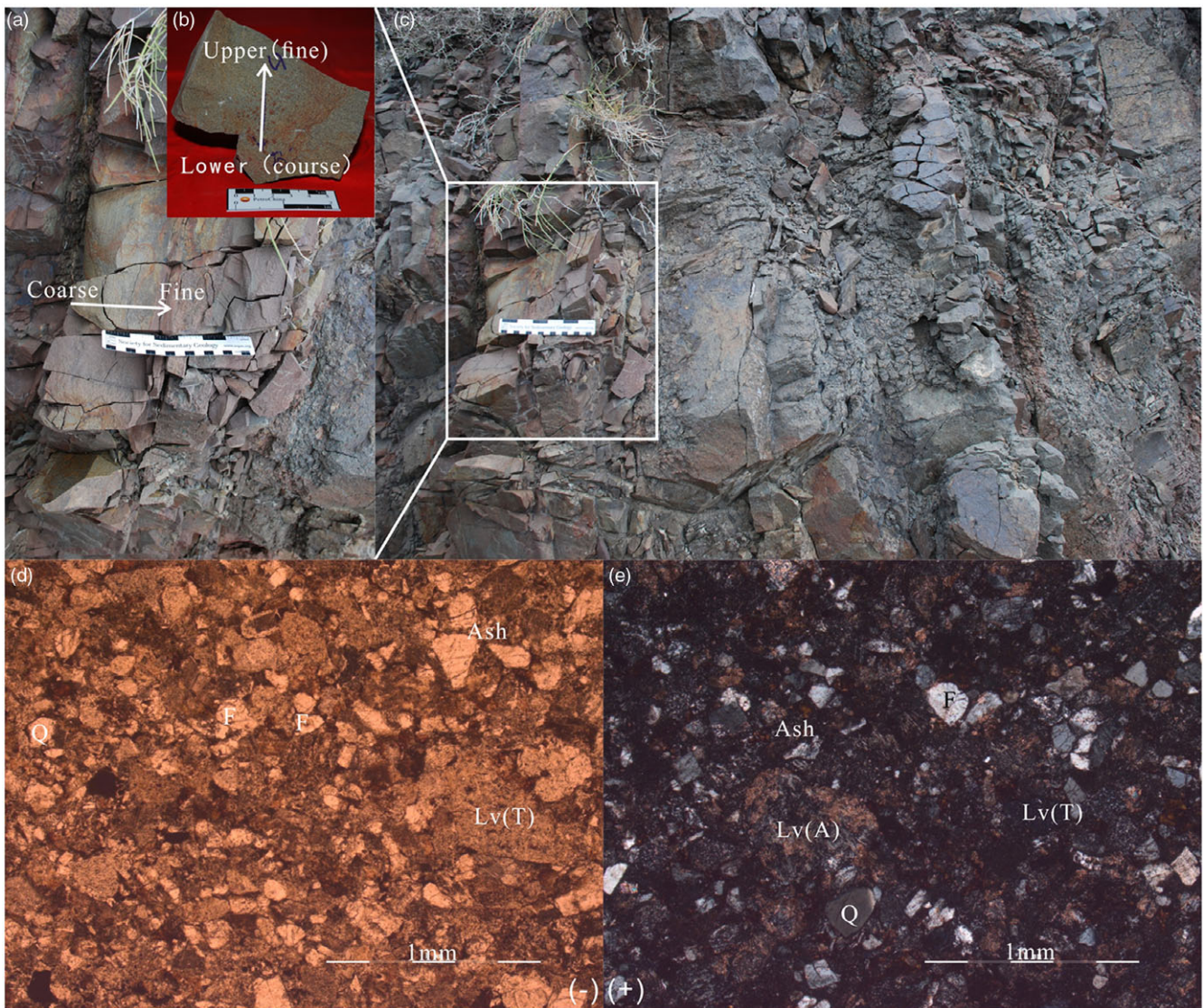
Fig. 3. (Colour online) (a–c) Field photographs of the Aladeyikesai Formation on Hala'alat Mountain. (d, e) Photomicrographs of selected sandstone samples under (d) plane-polarized and (e) cross-polarized light. Abbreviations of minerals: A – andesite; Ash – volcanic ash; F – feldspar; Lv – volcanic lithic fragment; Q – quartz; T – tuff.

with depositional ages (Dickinson & Gehrels, 2009). The mean age YC1σ(2+) of the youngest cluster (n ≥ 2) of grains that have overlapping ages at 1σ has higher accuracy (Zhao et al. 2020); thus, we use YC1σ(2+) to evaluate the MDA. In addition, if the sediment came from simultaneous continuous volcanic activity, the MDA can usually effectively define the depositional age of the stratum (Dickinson & Gehrels, 2009).

Based on detrital samples from this study, the MDAs (YSG, YPP, YC1σ(2+) and YC2σ(3+)) are calculated, and the results are shown in Table 3 and Figure 6. The YC1σ(2+) of the Hala'alat Formation sandstone is 314.6 ± 1.54 Ma (Fig. 6b), indicating that the rock was not deposited earlier than the Moscovian in the late Carboniferous period, which is consistent with the ages of rhyolite (304.5 ± 3.1 Ma) and pyroxene andesite (306.9 ± 5.5 Ma) in this stratum (Li, G.Y. et al. 2015). The YC1σ(2+) of the Aladeyikesai Formation sandstone is 330.8 ± 0.61 Ma (Fig. 6a), indicating that the stratum depositional time was not earlier than the Serpukhovian in the early

Carboniferous period, which is consistent with the absolute age measured from basalt (303.8 ± 2.4 Ma, Xiang, 2015) and the relative age represented by palaeontological fossils (late Carboniferous, Kasimovian, Peng et al. 2016).

Theoretically, the weighted average age of the youngest zircon in the Aladeyikesai Formation should be less than that in the Hala'alat Formation, but the test results show the opposite.

According to the geological background of the study area, volcanic activity was occurring during the deposition of the Hala'alat Formation (Zong et al. 2014; Li, G. Y. et al. 2016), and a tuffaceous composition accounts for a large proportion. Most detrital zircons likely came from effusive rocks in the same sedimentary period, and the provenance was relatively singular. However, the Aladeyikesai Formation is dominated by neritic terrigenous clastic rocks (Gong & Zong, 2015; Peng et al. 2016), and detrital zircons are mainly from old surrounding sedimentary strata. Therefore, the MDA of the Hala'alat Formation provides a better constraint than that of the Aladeyikesai Formation.

Table 2. Mass percentages of heavy minerals in the upper Carboniferous samples from Hala'alat Mountain (%)

Formation	Sample no.	Leucoxene	Magnetite	Zircon	Cr-spinel	Chromite	Allanite	Pyroxene	Hornblende	Apatite	Epidote	Garnet	Ilmenite
C_2a	S8-4	64.7		1.3	28.8				0.2	4.6		0.4	
C_2h	S9-1		12.6	0.3		1.4		1.4	4.8	0.5	47.2	0.5	31.3
	S9-3		34.2	0.2		2.6	0.4	1.2	11.3	0.04	25.7	1.0	23.3
	S10-2		0.1	0.03				97.5		0.1	2.3		

6.b. Provenance analysis

Owing to the complex provenance system of the sedimentary basin and the wide distribution of igneous rocks in the same period, it is difficult to explore the provenance of the upper Carboniferous rocks in the HLM area. Therefore, it is necessary to compare evidence, such as petrological characteristics, chronological characteristics, heavy mineral assemblages and palaeocurrents, with the potential provenance area to more accurately locate the provenance area and assess the tectonic evolution.

6.b.1. Parent rock properties of the provenance area

It is necessary to determine the parent rock properties and potential source areas based on information from heavy mineral assemblages. Iron, titanium, chromium and other metal deposits are often associated with basic igneous rocks (Tian, 2015), while magnetite, ilmenite and chromite are abundant in the upper Carboniferous sandstone samples of the HLM area. Moreover, some Cr-spinel and pyroxene are present. Combined with a large amount of andesite debris and a small amount of gabbro-diabase debris, as observed under the microscope, these results indicate that the parent rocks are mainly intermediate-basic igneous rocks. The pyroclastic rock samples of the Hala'alat Formation also show that they are mainly andesite-basalt breccia with a large amount of pyroxene and a small amount of serpentine, which also corroborates the hypothesis. On the other hand, the upper Carboniferous samples contain a small amount of automorphic–subautomorphic magmatic zircons. Combined with a certain amount of apatite, intermediate-acidic igneous rocks may be the parent rocks.

The epidote content in the sandstone samples of the Hala'alat Formation is higher. The epidote not only has a metasomatic metamorphic origin but also a magmatic origin. The former may be related to epidotization when igneous rock intrudes the surrounding rock, and the latter is mainly produced in calc-alkaline granitic rocks (Zhao *et al.* 2019). The ophiolitic mélange is also subject to alteration and provides minerals such as serpentine, zoisite or epidote (Chen *et al.* 2008; Zhao *et al.* 2013). Zhao *et al.* (2019) studied epidote in the Triassic heavy minerals in the northwestern Mahu Sag, Junggar Basin, and believed that it was mainly magmatic epidote and that the parent rock was probably intermediate-acidic igneous rock in West Junggar. The epidote may be inherited in the upper Carboniferous in adjacent sedimentary areas. Considering the limited distribution of metamorphic rocks in West Junggar, these minerals are more likely to come from intermediate-acidic igneous rocks.

Based on the heavy mineral assemblage reported here, the parent rocks of the upper Carboniferous strata in the HLM area are likely mainly intermediate-basic igneous rocks followed by intermediate-acidic igneous rocks (Table 4). According to the distribution of strata around the HLM area, andesite, basalt and tuff are widely distributed throughout West Junggar. Granite also intrudes into each tectonic unit. Ophiolitic mélange and intermediate-basic dykes are also well developed. All of these igneous rocks may be potential sources. Therefore, the provenance cannot be identified only by heavy mineral assemblages. It is necessary to clarify the stratigraphic distribution characteristics and chronological framework of potential provenance areas and combine heavy mineral information with zircon U–Pb chronology to comprehensively investigate the provenance.

Notably, the sample size of the heavy mineral analysis is limited. Considering the size-sorting effect of coarse clastic rocks, the conclusions derived from the parent rock properties indicated by the
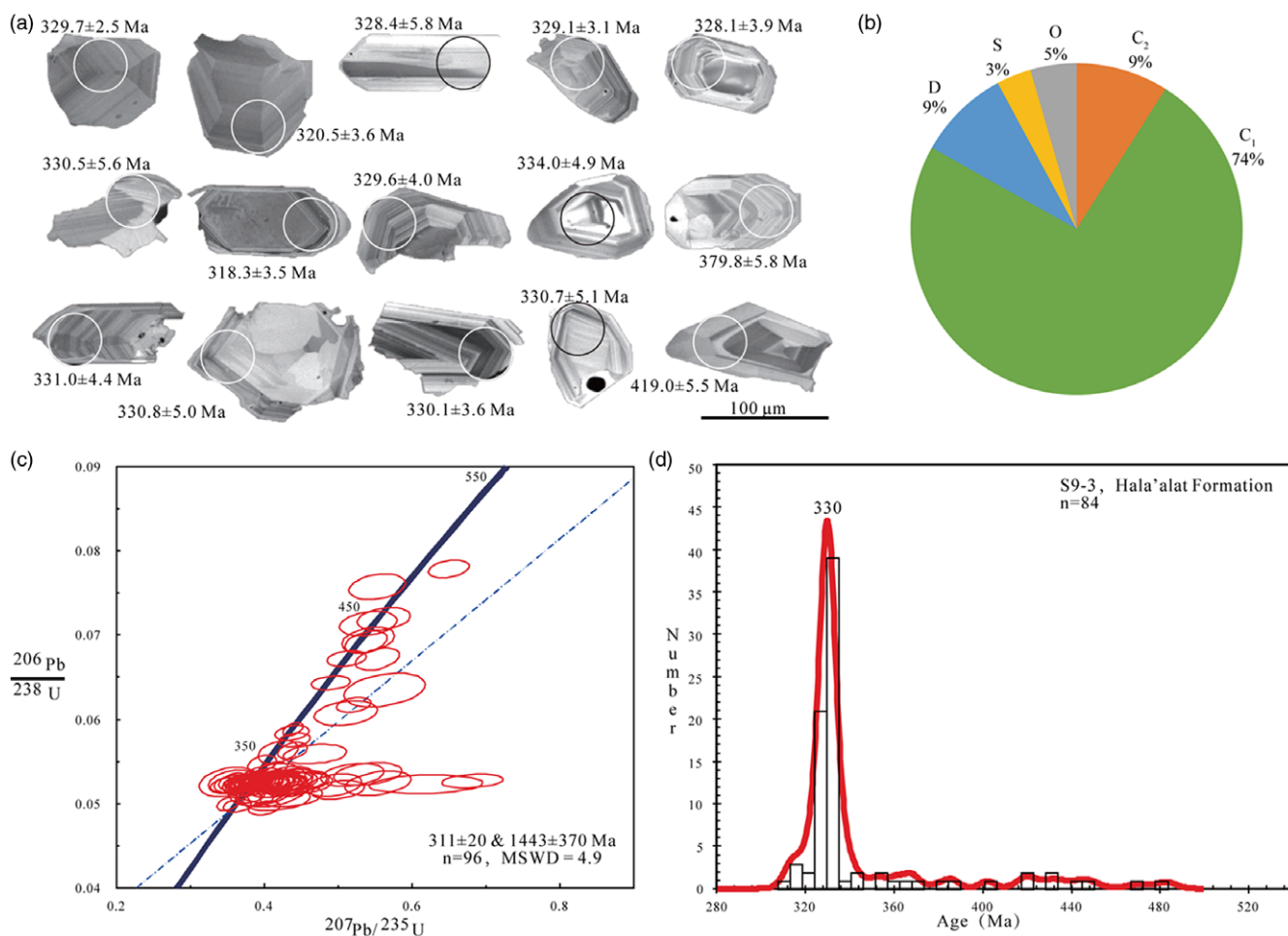
Fig. 4. (Colour online) Zircon dating results of the sandstones from the Hala'alat Formation on Hala'alat Mountain. (a) Cathodoluminescence photographs. (b) Pie chart of ages. Note that the stratigraphic age division is based on the International Chronostratigraphic Chart (2020) (Cohen *et al.* 2013, updated). (c) U–Pb age concordia diagram. (d) Histogram of the age distribution.

heavy mineral assemblages in this study should be cautious. The conclusions need the support of more samples or other experimental data, such as mudstone geochemistry characteristics.

6.b.2. Provenance locations and related rock types

Tao *et al.* (2013) measured the palaeocurrent directions of 23 groups of foreset laminae of the Hala'alat Formation sandstone in the HLM area, revealing two provenances, namely, provenances from the south and north, during the late Carboniferous period, and the northern provenance contributed more to sedimentation. Their study is helpful for inferring the provenance locations in this paper.

The main peak age of the Hala'alat Formation sandstone is similar to that of the Aladeyikesai Formation sandstone, which is 330 Ma; this age accounts for the highest proportion of all age data, indicating that early Carboniferous igneous rocks are the main source. The igneous rocks with this peak age are mainly distributed in three regions throughout West Junggar: (1) Granite bodies extensively intruded into the Tarbgatay, E'min and Saur mountains to the north of the HLM area (this area is part of the late Palaeozoic ZhSA) at 335–320 Ma in the early Carboniferous period (Choulet *et al.* 2012*a*; Gao *et al.* 2014; Jin, 2016; Zhang *et al.* 2017; Zhang, C. *et al.* 2018). (2) The western sections of Xiemisitai Mountain and Saier Mountain

in the BCA mainly contain early Carboniferous intermediate-acidic effusive rocks, and the zircon U–Pb ages are 331 ± 2.4 Ma (dacite) (Yi *et al.* 2014) and 331 ± 9 Ma (basalt) (Geng *et al.* 2011). (3) The zircon U–Pb ages of the HLM–ZRM area (i.e. late Palaeozoic DTMB) are 345–325 Ma, and the lithology is mostly basalt, andesite, tuff (Xu *et al.* 2012) and granite intrusions (Duan *et al.* 2019). Li, D. *et al.* (2015) suggested that during early Devonian – early Carboniferous times, the ZhSA was combined with the BCA and Junggar terrane, and the ZhSA and HLM were divided by the BCA (Zhang, 2020), which may have been unfavourable for the transport of sediments from the ZhSA to HLM. As mentioned in Sections 3.a, 3.b and 5.a, the sedimentation in the study area occurred near the source, and Tao *et al.* (2013) suggested that the northern provenance supplied more sediments than the southern provenance. In addition, the zircons developed in the mafic rocks are usually rare and small; therefore, the method of detrital zircon U–Pb dating is biased to reflect more contributions of the felsic rocks. Based on the above discussion, the early Carboniferous intermediate-acidic effusive rocks distributed in the BCA were likely the primary source, and the early Carboniferous intermediate-acidic igneous rocks of the DTMB were likely the secondary source, but the presence of detrital fragments originating from the ZhSA cannot be excluded.

Table 3. Age comparisons of the youngest detrital zircons from different upper Carboniferous units in the Hala'alat Mountain area

Formation	Sample No.	YSG (Ma)	YPP (Ma)	YC1σ(2+) (Ma)	YC2σ(3+) (Ma)
C$_2$a	S8-4	319.9 ± 3.51	331	330.8 ± 0.61	330.5 ± 0.6
C$_2$h	S9-3	311.6 ± 3.41	330	314.6 ± 1.54	316.3 ± 1.31

YSG – youngest single grain age; YPP – youngest graphical age peak controlled by more than one grain age; YC1σ(2+): youngest 1σ grain cluster – mean age of the youngest two or more grains that overlap in age at 1σ; YC2σ(3+): youngest 2σ grain cluster – mean age of the youngest three or more grains that overlap in age at 2σ.
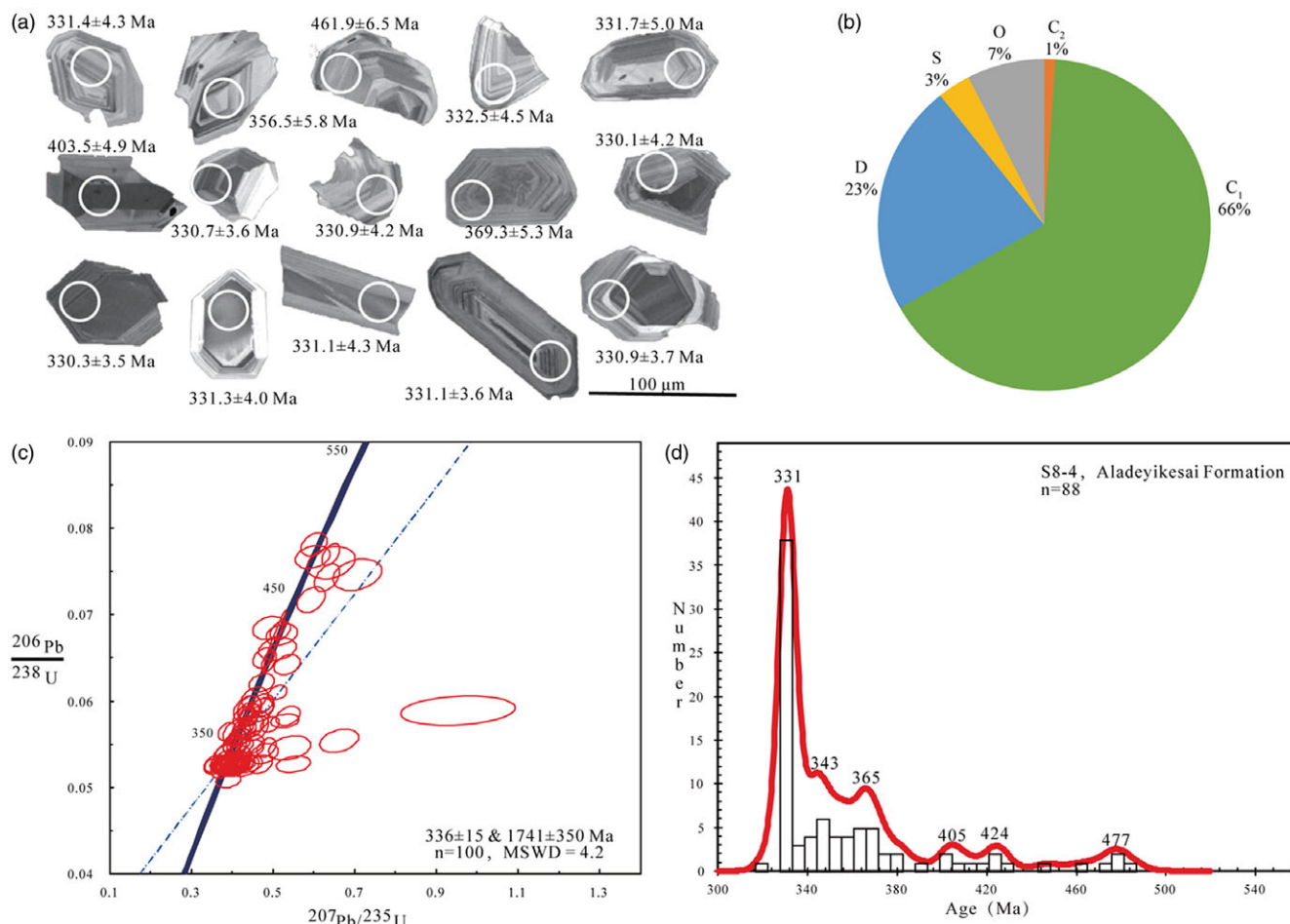

Fig. 5. (Colour online) Zircon dating results of the sandstones from the Aladeyikesai Formation on Hala'alat Mountain. (a) Cathodoluminescence photographs. (b) Pie chart of ages. Note that the stratigraphic age division is based on the International Chronostratigraphic Chart (2020) (Cohen *et al*. 2013, updated). (c) U–Pb age concordia diagram. (d) Histogram of the age distribution.

It is worth noting that the Junggar Ocean northwards-subducting basin system resulted in the formation of an island arc basin system, and several island arc systems of the late Palaeozoic are present beneath the Mesozoic–Cenozoic strata in the northern Junggar Basin (Li, D. *et al*. 2015). For example, Carboniferous island arc effusive rocks developed in the Zhongguai area on the NW margin and mainly include andesite, basalt and rhyolite (Li, D. *et al*. 2014; Li, D. *et al*. 2016). Therefore, combined with the south to north palaeocurrent data (Tao *et al*. 2013), these Carboniferous island arcs inside the basin in the southern part of the study area may have also provided some clastic sediments.

In addition to the main peak at 330 Ma, the sandstone of the Aladeyikesai Formation has multiple peaks. The detrital zircons with secondary peaks of 370–344 Ma (Late Devonian – early

Carboniferous) are consistent with the ages of intermediate-basic effusive rocks, intermediate-acidic intrusions and ophiolitic mélange in the DTMB. For example, the U–Pb age of zircon in andesite measured in the Sartohai area is 345.6 ± 6.2 Ma (Tong *et al*. 2009), in diorite is 344.4 ± 6.8 Ma (Geng *et al*. 2011) and in andesite is 344 ± 3 Ma (Geng *et al*. 2011); these areas are south of the Darbut Fault. The ages of the gabbro-diabase near the Darbut Fault vary from 347 Ma to 368 Ma (Chen *et al*. 2013; Tian, 2015; Yang *et al*. 2019). Therefore, multistage arc magmatism developed in the DTMB during 360–325 Ma (Xu, 2012); thus, the DTMB may have provided terrigenous clastic sediments.

Zircons with ages mainly within 427–404 Ma (late Silurian – Early Devonian) may be related to a series of Darbut Ophiolitic Mélange with zircon ages from 420 to 390 Ma that is present in this area (Xu *et al*. 2006; Gu *et al*. 2009; Li, G. *et al*. 2014), and
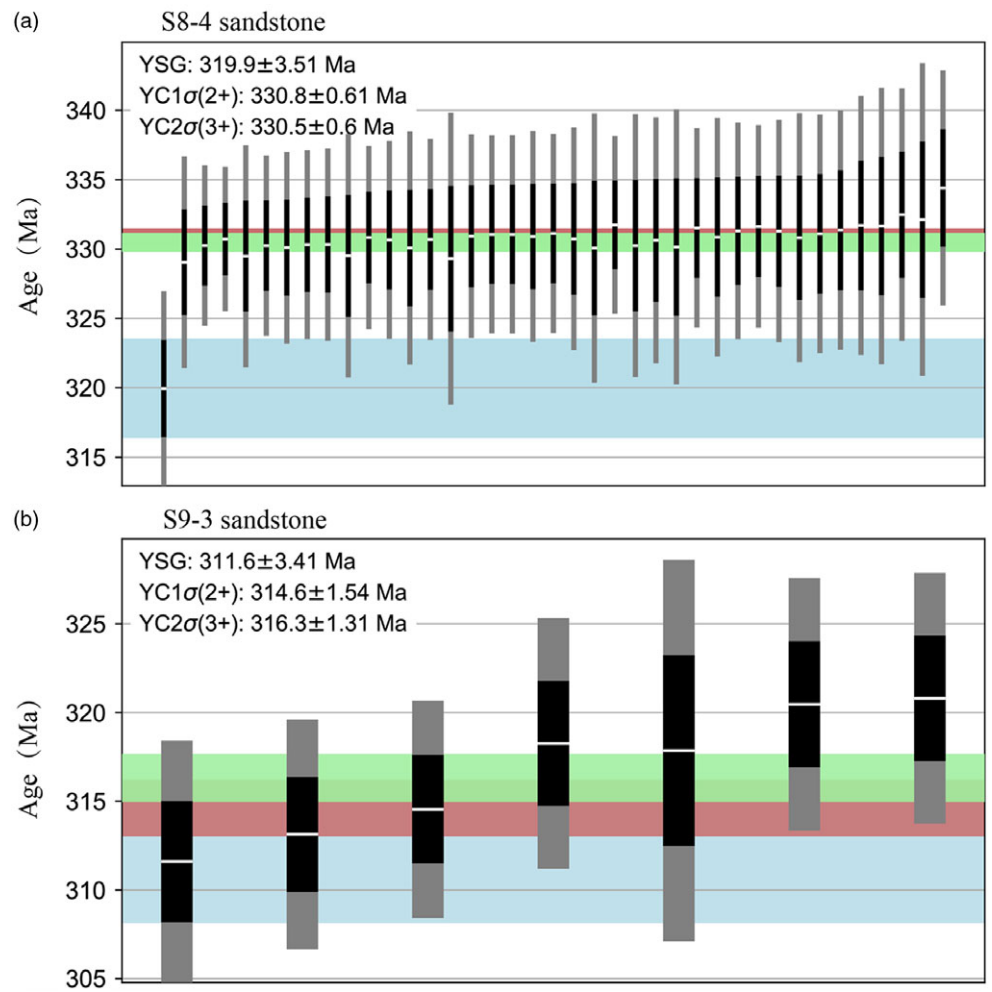
Fig. 6. (Colour online) Maximum depositional age of the upper Carboniferous strata of Hala'alat Mountain. (a) Aladeyikesai Formation sandstone. (b) Hala'alat Formation sandstone. Legend: blue (bottom) – youngest single grain age (YSG); red (middle) – weighted average age (YC1σ); green (top) – weighted average age (YC2σ); horizontal white bar – average age; vertical black bar – 1σ uncertainty; vertical grey bar – 2σ uncertainty.

intermediate-acidic igneous rocks from the BCA with ages of 430–390 Ma from the north may also be present (Chen *et al.* 2010; Zheng, B. *et al.* 2019). The latter are more likely the main source rocks.

The early Ordovician zircon ages of 478–476 Ma correspond better to the Honggululeng Ophiolitic Mélange (cumulate gabbro, 472 ± 8.4 Ma) (Zhang & Guo, 2010), E'min Ophiolitic Mélange (gabbro, 476 ± 2 Ma) (Zheng, R. G. *et al.* 2019) and Kujibai Ophiolitic Mélange (gabbro, 478.3 ± 3.3 Ma) (Zhu & Xu, 2006). The above ophiolites and the Hoboksar Ophiolitic Mélange (gabbro, 484 ± 3 Ma) on the north side formed during the same period (Du & Chen, 2017) and comprise a large E–W-striking ophiolitic mélange belt, indicating that the Ordovician zircons may have come from the KHOMB.

6.c. Provenance evolution

Previous studies have shown that (1) the sediments of the Xibekulas Formation in the HLM–ZRM area mainly came from igneous rocks, indicating that magmatic activity was high during early Carboniferous time in the peripheral Baogutu area (i.e. southeastern DTMB) and the Devonian System in the Tiechanggou area (i.e. northwestern DTMB) in the north, and a small number of older zircons came from the Mayile Ophiolitic Mélange and the adjacent Ordovician–Silurian strata (i.e. southern West Junggar) (Zhang *et al.* 2015; An *et al.* 2019). (2) The sources

of the Baogutu Formation were probably the Middle Devonian and early Carboniferous intermediate-acidic effusive rocks and the middle Silurian Mayile ophiolitic mélange in the Barleik Mountain area (Liao *et al.* 2015). (3) The clastic source of the Telegula Formation may mainly be from the early Carboniferous intermediate-acidic island arc effusive rocks in the western margin of HLM and Xiemisitai Mountain (Liao *et al.* 2015; Zhang *et al.* 2015). (4) The potential provenances of the Hala'alat Formation were primarily related to the early Carboniferous intermediate-acidic effusive rocks of the BCA, and the secondary provenances were the early Carboniferous intermediate-acidic igneous rocks distributed in the DTMB and the early Carboniferous island arc in the basin. In addition, a few detrital fragments might originate from the ZhSA. (5) The Aladeyikesai Formation inherited the provenance system of the Hala'alat Formation and mixed with the provenance of the late Devonian – early Carboniferous igneous rocks in the DTMB, the Silurian–Devonian intermediate-acidic igneous rocks from the BCA and the Ordovician KHOMB.

According to the comparative analysis (Fig. 7a), the source of the upper Carboniferous Hala'alat Formation in the HLM area is relatively singular. The main zircon age peak of the Aladeyikesai Formation is similar to that of the Hala'alat Formation, with similar petrology, indicating that the provenance system has a certain inheritance. Several robust peaks are in the age range of 427–344 Ma, and the proportion of measuring points

Table 4. Heavy mineral classifications and characteristics of the upper Carboniferous samples from Hala'alat Mountain

| Formation	Main minerals (>10 %)	Secondary minerals (1–10 %)	Minor minerals (≤1 %)	Parent rock properties
C_2a	Leucoxene, Cr-spinel	Apatite, zircon	Garnet, hornblende	Mainly intermediate-basic igneous rocks followed by intermediate-acidic igneous rocks
C_2h	Epidote, ilmenite, magnetite	Hornblende, chromite, pyroxene	Garnet, zircon, apatite, epidote	Mainly intermediate-basic igneous rocks followed by intermediate-acidic igneous rocks
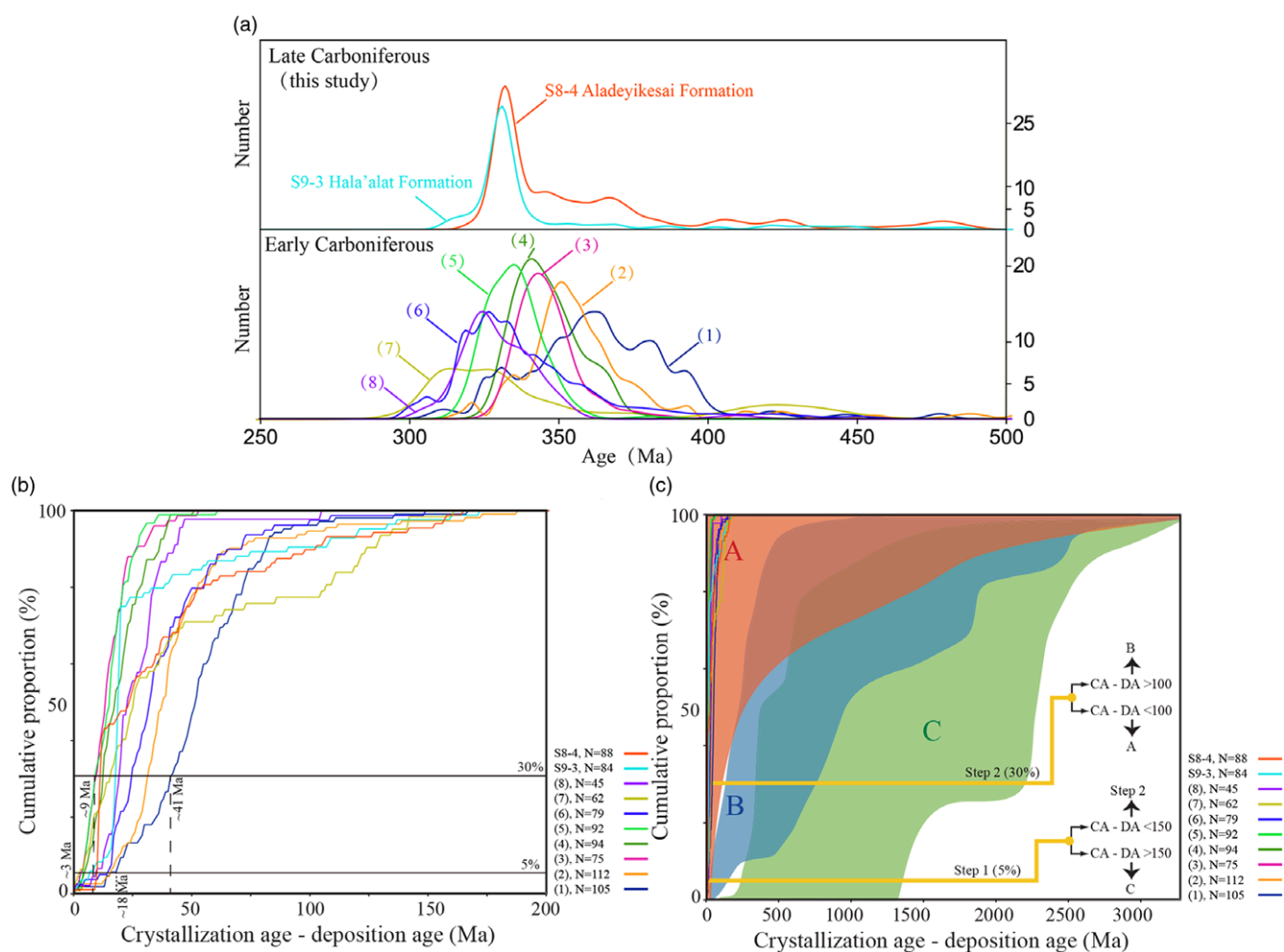
Fig. 7. (Colour online) (a) Probability density plots of detrital zircon U–Pb ages of the Carboniferous sedimentary rocks in the Hala'alat–Zaire mountains, West Junggar. (b) The cumulative proportion curves based on the differentia between the crystallization ages of detrital zircons and deposition ages of the samples. (c) Model of the cumulative proportion curves of detrital zircons in different tectonic settings (Cawood *et al.* 2012). A – convergent settings; B – collisional settings; C – extensional settings. Detrital zircon age data adapted from the (1) Xibekulas Formation (Zhang *et al.* 2015); (2) Xibekulas Formation (An *et al.* 2019); (3) Xibekulas Formation (Chen *et al.* 2013); (4) Xibekulas Formation (Zhang *et al.* 2021); (5) Baogutu Formation (Zhang *et al.* 2021); (6) Telegula Formation (Zhang, P. *et al.* 2018); (7) Telegula Formation (Choulet *et al.* 2012b); (8) Telegula Formation (Zhang, P. *et al.* 2018); and S8-4, S9-3 (this study).

increases. It is possible that during late Carboniferous time, the closure of the Junggar Ocean uplifted the older strata of the BCA and the DTMB to the surface and caused denudation. The age distribution also includes some early Ordovician ages (480–475 Ma), indicating that the provenance area extends northwards to the KHOMB.

Additionally, for the Carboniferous sedimentary samples in the Hala'alat–Zaire mountains, calculations are made to determine the difference between the measured crystallization age for a detrital zircon grain and the depositional age of the succession in which it occurs, plotted as cumulative proportion curves (Fig. 7b).

Cawood *et al.* (2012) established detrital zircon spectra with different age distribution patterns reflect the sedimentary tectonic environment. Convergent plate margins are characterized by a single age peak with a similar synsedimentary age. Using this pattern, the depositional ages are very similar to the crystallization ages of the major detrital zircons, which is a typical feature of arc-related basins (Fig. 7c). The tectonic background in which the Hala'alat and Zaire mountains formed was a convergent setting during Carboniferous time (Cawood *et al.* 2012).

Considering that the proximal sedimentation is obviously controlled by the regional tectonic pattern, the change in the detrital
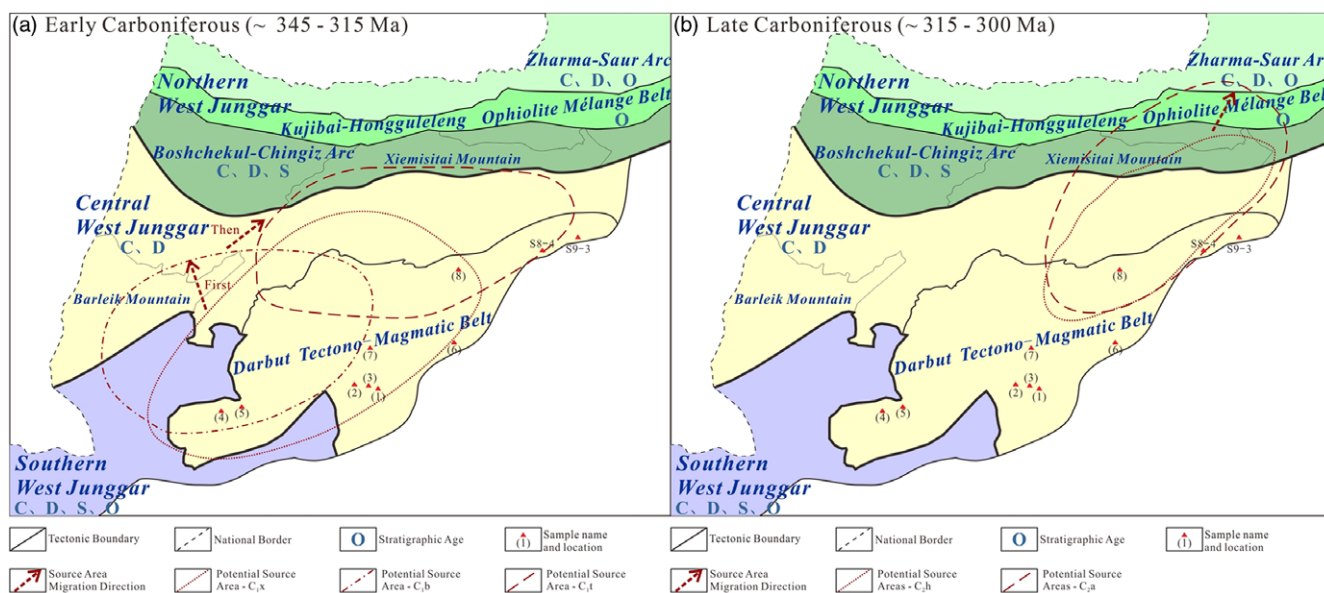
Fig. 8. (Colour online) Schematic map of potential Carboniferous source areas in the Hala'alat–Zaire mountains area showing that the source regions migrated northeastwards from the Barleik Mountain area to the Xiemisitai Mountain area from the (a) early to (b) late Carboniferous period. Note: The West Junggar terrane is subdivided into northern, central and southern parts in different colours. The northern West Junggar comprises the ZhSA, KHOMB and BCA. The tectonic boundaries are simplified from Figure 1. The samples are from the DTMB (see data sources in Fig. 7). The capital letters indicate the potential parent rock ages in each tectonic unit.

zircon age distribution in the sedimentary area has a certain indicative value for the tectonic evolutionary history. Based on the analysis, the source regions of the HLM–ZRM area migrated northeastwards from the Barleik Mountain area to the Xiemisitai Mountain area from early to late Carboniferous times (Fig. 8). This migration may be related to the regional tectonic activities in the same period: as the residual ocean basin was gradually filled, the Carboniferous seawater in the middle of West Junggar retreated from southwest to northeast to the HLM area, and the depocentre also migrated from south to north and from west to east; these processes are almost consistent with research results reported by Zong *et al.* (2014), Gong & Zong (2015), Liao *et al.* (2015) and Zhang *et al.* (2015).

7. Conclusions

Through provenance analysis, this study determined the parent rock properties and age composition of the upper Carboniferous sedimentary strata in the HLM area, thereby providing a basis for further characterizing the sediment transport path and tectonic sequence – sedimentary response and evolutionary history of the whole Junggar Basin.

(1) To determine the timing for the formation of upper Carboniferous strata in the Hala'alat Mountain area, YC1σ(2+) age is selected to evaluate the MDA. The Hala'alat and Aladeyikesai formations sandstones show YC1σ(2+) ages of 314.6 ± 1.54 Ma and 330.8 ± 0.61 Ma, respectively. The U–Pb age derived from the Aladeyikesai Formation is greater than that of the underlying Hala'alat Formation, so it cannot be used to constrain the MDA.

(2) The sandstone petrology of the Hala'alat Formation sandstone on HLM reveals that its provenance is proximal to the deposits, including angular to subangular grains, rich volcanic lithic fragments, and an immature to submature composition and texture. The main heavy minerals include magnetite, epidote,

ilmenite and hornblende. It is likely that the primary parent rocks are mainly intermediate-basic igneous rocks, and the minor parent rocks are local intermediate-acidic igneous rocks. The zircon age spectrum has only one main peak (330 Ma), indicating that the sediments mainly came from the early Carboniferous intermediate-acidic effusive rocks of the BCA, and the secondary sources were the early Carboniferous intermediate-acidic igneous rocks distributed in the DTMB and the early Carboniferous island arc in the basin. In addition, a few detrital fragments might originate from the ZhSA.

(3) The petrological characteristics of the Aladeyikesai Formation sandstone are similar to those of the Hala'alat Formation, indicating that the formations both had proximal sedimentation. The heavy mineral assemblage is leucoxene–Cr-spinel–apatite. It is likely that the parent rocks were mainly intermediate-basic igneous rocks, followed by intermediate-acidic igneous rocks. The main peak value of the zircon age spectrum is 331 Ma, and the sandstone likely inherited the provenance system of the Hala'alat Formation. Several secondary peaks at 370–344 Ma, 427–404 Ma and 478–476 Ma indicate that they may have come from the late Devonian – early Carboniferous igneous rocks in the DTMB, the Silurian–Devonian intermediate-acidic igneous rocks from the BCA and the Ordovician KHOMB, respectively.

(4) The provenance of the upper Carboniferous Hala'alat Formation in the HLM–ZRM area is generally singular, while the provenance system of the Aladeyikesai Formation has a certain inheritance. Moreover, the closure of the Junggar Ocean during late Carboniferous time caused the older strata in the BCA and the DTMB to be uplifted to the surface and denuded. Also, the provenance area extends northwards to the KHOMB.

(5) From early Carboniferous to late Carboniferous times, the potential source areas in the HLM–ZRM area migrated northeastwards from the Barleik Mountain area to the Xiemisitai

Mountain area, which may be related to the tectonic activities in the same period. As the residual ocean basin was gradually filled, the Carboniferous seawater in the middle of West Junggar retreated from southwest to northeast to the HLM area, and the depocentre also moved from south to north and from west to east.

References

An F, Wei SN, Fang ZK, Zheng B and Deng Y (2019) Petrology and zircon U–Pb geochronology of tuffaceous conglomerate in the Xibeikulasi Formation, West Junggar, and its implication for sedimentary sequence. *Acta Geologica Sinica* **93**, 1954–67 (in Chinese with English abstract).

Andersen T (2002) Correction of common lead in U–Pb analyses that do not report Pb-204. *Chemical Geology* **192**, 59–79. doi: 10.1016/s0009-2541(02)00195-x.

Belousova EA, Griffin WL, O'Reilly SY and Fisher NI (2002) Apatite as an indicator mineral for mineral exploration: trace-element compositions and their relationship to host rock type. *Journal of Geochemical Exploration* **76**, 45–69.

Cawood PA, Hawkesworth CJ and Dhuime B (2012) Detrital zircon record and tectonic setting. *Geology* **40**, 875–8.

Chen B, Zhu YF, Wei SN and Xu X (2008) Garnet amphibolite found in Keramay ophiolitic melange, western Junggar, NW China. *Acta Petrologica Sinica* **24**, 1034–40 (in Chinese with English abstract).

Chen JF, Han BF, Ji JQ, Zhang L, Xu Z, He GQ and Wang T (2010) Zircon U–Pb ages and tectonic implications of Paleozoic plutons in northern West Junggar, North Xinjiang, China. *Lithos* **115**, 137–52.

Chen S, Guo ZJ, Pe-Piper G and Zhu BB (2013) Late Paleozoic peperites in West Junggar, China, and how they constrain regional tectonic and palaeoenvironmental setting. *Gondwana Research* **23**, 666–81.

Choulet F, Cluzel D, Faure M, Lin W, Wang B, Chen Y, Wu FY and Ji WB (2012a) New constraints on the pre-Permian continental crust growth of Central Asia (West Junggar, China) by U–Pb and Hf isotopic data from detrital zircon. *Terra Nova* **24**, 189–98.

Choulet F, Faure M, Cluzel D, Chen Y, Lin W and Wang B (2012b) From oblique accretion to transpression in the evolution of the Altaid collage: new insights from West Junggar, northwestern China. *Gondwana Research* **21**, 530–47.

Cohen KM, Finney SC, Gibbard PL and Fan JX (2013, updated 2020) The International Chronostratigraphic Chart. *Episodes* **36**, 199–204.

Dickinson WR and Gehrels GE (2009) Insights into North American paleogeography and paleotectonics from U–Pb ages of detrital zircons in Mesozoic strata of the Colorado Plateau, USA. *International Journal of Earth Sciences* **99**, 1247–65.

Du HY and Chen JF (2017) The determination of Hoboksar ancient oceanic basin in West Junngar: evidence from zircon U–Pb age and geochemistry of the Hoboksar ophiolitic mélange. *Acta Geologica Sinica* **91**, 2638–50 (in Chinese with English abstract).

Duan FH, Li YJ, Zhi Q, Yang GX and Gao JB (2019) Petrogenesis and geodynamic implications of Late Carboniferous sanukitic dikes from the Bieluagaxi area of West Junggar, NW China. *Journal of Asian Earth Sciences* **175**, 158–77.

Gao R, Xiao L, Pirajno F, Wang GC, He XX, Yang G and Yan SW (2014) Carboniferous–Permian extensive magmatism in the West Junggar, Xinjiang, northwestern China: its geochemistry, geochronology, and petrogenesis. *Lithos* **204**, 125–43.

Gao R, Xiao L, Wang GC, He XX, Yang G and Yan SW (2013) Paleozoic magmatism and tectonic setting in West Junggar. *Acta Petrologica Sinica* **29**, 3413–34 (in Chinese with English abstract).

Gehrels G (2014) Detrital zircon U–Pb geochronology applied to tectonics. *Annual Review of Earth and Planetary Sciences* **42**, 127–49.

Geng HY, Sun M, Yuan C, Zhao GC and Xiao WJ (2011) Geochemical and geochronological study of Early Carboniferous volcanic rocks from the West Junggar: petrogenesis and tectonic implications. *Journal of Asian Earth Sciences* **42**, 854–66.

Gong YM and Zong RW (2015) Paleozoic stratigraphic regionalization and paleogeographic evolution in West Junggar, Northwestern China. *Earth Science* **40**, 461–84 (in Chinese with English abstract).

Gu PY, Li YJ, Zhang B, Tong L and Wang JN (2009) LA-ICP-MS zircon U–Pb dating of gabbro in the Darbut ophiolite, western Junggar, China. *Acta Petrologica Sinica* **25**, 1364–72 (in Chinese with English abstract).

Guo LS, Liu YL, Wang ZH, Song D, Xu FJ and Su L (2010) The zircon U–Pb LA-ICP-MS geochronology of volcanic rocks in Baogutu areas, western Junggar. *Acta Petrologica Sinica* **26**, 471–7 (in Chinese with English abstract).

Jian P, Li DY, Shi YR and Zhang FQ (2005) SHRIMP dating of SSZ ophiolites from northern Xinjiang Province, China: implications for generation of oceanic crust in the Central Asian Orogenic Belt. In *Structural and Tectonic Correlation Across the Central Asian Orogenic Collage: Northeastern Segment* (ed. EV Sklyarov), pp. 246–51. Irkutsk: Institute of the Earth's Crust, Siberian Branch of the Russian Academy of Sciences.

Jin S (2016) *Study on geochronology and geochemistry of Paleozoic magmatism in West Junggar area, Xinjiang.* Ph.D. thesis, China University of Geosciences, Wuhan, China. Published thesis (in Chinese with English abstract).

Li D, He D, Lian Y, Lu Y and Yi Z (2016) Structural evolution and Late Carboniferous magmatism of the Zhongguai arc in the western Junggar Basin, Northwest China: implications for tectonic evolution of the Junggar Ocean. *International Geology Review* **59**, 1234–55.

Li D, He DF, Santosh M and Ma DL (2015) Tectonic framework of the northern Junggar Basin Part II: the island arc basin system of the western Luliang Uplift and its link with the West Junggar terrane. *Gondwana Research* **27**, 1110–30.

Li D, He DF, Yang YH and Lian YC (2014) Petrogenesis of mid-Carboniferous volcanics and granitic intrusions from western Junggar Basin boreholes: geodynamic implications for the Central Asian Orogenic Belt in Northwest China. *International Geology Review* **56**, 1668–90.

Li G, Yang B, Liang EY, Ma TQ and Cao SH (2014) SHRIMP zircon U–Pb age and geochemical characteristics of mafic rock from Liushugou-Darbut in western Junggar, Xinjiang, China. *Geology and Mineral Resources of South China* **30**, 194–205 (in Chinese with English abstract).

Li GY, Li YJ, Wang R, Yang GX, Xiang KP, Liu J and Li Z (2015) Zircon LA-ICP-MS U–Pb dating of volcanics in Hala'alate Formation of western Junggar. *Northwestern Geology* **48**, 12–21 (in Chinese with English abstract).

Li GY, Li YJ, Xiang KP, Wang R, Liu J, Li Z and Yang GX (2016) Revision and regional correlation of the Hala'alate Formation in western Junggar Basin. *Journal of Stratigraphy* **40**, 76–84 (in Chinese with English abstract).

Li HQ, Chen FW and Cai H (2000) Study on Rb–Sr isotopic ages of gold deposits in West Junggar area, Xinjiang. *Acta Geologica Sinica* **74**, 181–92 (in Chinese with English abstract).

Liao WL, Xiao L, Zhang L and Wang GC (2015) Provenance and tectonic settings of Early Carboniferous sedimentary strata in western Junggar, Xinjiang. *Earth Science* **40**, 485–503 (in Chinese with English abstract).

Liu B, Han BF, Chen JF, Ren R, Zheng B, Wang ZZ and Feng LX (2017) Closure time of the Junggar-Balkhash Ocean: constraints from late Paleozoic volcano-sedimentary sequences in the Barleik Mountains, West Junggar, NW China. *Tectonics* **36**, 2823–45.

Ma FH (2018) Geochemical and organic features of black shale in Tailegula Formation within Upper Carboniferous, Halaalate Mountain. *Xinjiang Geology* **36**, 507–12 (in Chinese with English abstract).

Peng XP, Li YJ, Li WD, Xiang KP, Li GY and Li Z (2016) The stratigraphic sequence, fossil assemblage and sedimentary environment of Aladeyikesai Formation in Hala'alate Mountain, West Junggar. *Xinjiang Geology* **34**, 297–301 (in Chinese with English abstract).

Qiao G and Zhao HS (2020) The redefinition of the Carboniferous strata in the Baobei area of western Junggar, Tuoli County, Xinjiang: evidence from zircon U–Pb dating. *Geology in China* **47**, 885–7 (in Chinese with English abstract).

Sharman GR, Sharman JP and Sylvester Z (2018) detritalPy: a Python-based toolset for visualizing and analysing detrital geo-thermochronologic data. *Depositional Record* **4**, 202–15.

Tao HF, Qiu Z, Ji HJ and Qiu JL (2017) Sedimentary environment and organic carbon enrichment factors of the Late Carboniferous Hala'alat hydrocarbon source rocks in West Junggar. *Chinese Journal of Geology* **52**, 79–92 (in Chinese with English abstract).

Tao HF, Wang QC, Yang XF and Jiang L (2013) Provenance and tectonic setting of Late Carboniferous clastic rocks in West Junggar, Xinjiang, China: a case from the Hala-alat Mountains. *Journal of Asian Earth Sciences* **64**, 210–22.

Tian YZ (2015) *Genesis of high-Al chromitite of the Sartohay ophiolite, Xinjiang*. Ph.D. thesis, Chinese Academy of Geological Sciences, Beijing, China. Published thesis (in Chinese with English abstract).

Tong LL, Li YJ, Zhang B, Liu J, Pang ZJ and Wang JN (2009) Zircon LA-ICP-MS U–Pb dating and geologic age of the Baogutu Formation andesite in the south of Daerbute faulted zone, western Junggar. *Xinjiang Geology* **27**, 226–30 (in Chinese with English abstract).

Wang R and Zhu YF (2007) Geology of the Baobei gold deposit in western Junggar and zircon SHRIMP age of its wall-rocks, western Junggar (Xinjiang, NW China). *Geological Journal of China Universities* **13**, 590–602 (in Chinese with English abstract).

Wang YJ, Jin YG and Jiang NY (1987) The age and paleoenvironmental characteristics of the Halaalate Formation. *Journal of Stratigraphy* **11**, 53–7 (in Chinese with English abstract).

Wei JM (1983) The Carboniferous marine bivalve fauna fossils in Halaalate Mountain, northwestern of Junggar Basin. *Xinjiang Petroleum Geology* **4**, 59–73 (in Chinese with English abstract).

Windley BF, Alexeiev D, Xiao WJ, Kroner A and Badarch G (2007) Tectonic models for accretion of the Central Asian Orogenic Belt. *Journal of the Geological Society, London* **164**, 31–47.

Xiang KP (2015) *Carboniferous sedimentary basin analysis and tectonic significance in the Baogutu-Halaalate Mountain, Western Junggar, Xinjiang*. Ph.D. thesis, Chang'an University, Xi'an, China. Published thesis (in Chinese with English abstract).

Xiang KP, Li YJ, Xu L, Zhang HW and Tong LL (2013a) Discussing the application of "Tailegula Formation" in Baogutu-Hatu region, West Junggar, XinJiang. *Xinjiang Geology* **31**, 148–52 (in Chinese with English abstract).

Xiang KP, Li YJ, Xu L, Zhang HW and Tong LL (2013b) The definition of Chengjisihanshan Formation and its significances in Baijiantan region, West Junggar, Xinjiang. *Northwestern Geology* **46**, 63–8 (in Chinese with English abstract).

Xiao WJ, Han CM, Yuan C, Sun M, Lin SF, Chen HL, Li ZL, Li JL and Sun S (2008) Middle Cambrian to Permian subduction-related accretionary orogenesis of Northern Xinjiang, NW China: implications for the tectonic evolution of central Asia. *Journal of Asian Earth Sciences* **32**, 102–17.

Xu X, He GQ, Li HQ, Ding TF, Liu XY and Mei SW (2006) Basic characteristics of the Karamay ophiolitic mélange, Xinjiang, and its zircon SHRIMP dating. *Geology in China* **33**, 470–5 (in Chinese with English abstract).

Xu Z (2012) *Paleozoic intra-oceanic subduction-accretion process in Mayile and Barleik Mountains in West Junggar, Xinjiang*. Ph.D. thesis, Peking University, Beijing, China. Published thesis (in Chinese with English abstract).

Xu Z, Han BF, Ren R, Zhou YZ and Su L (2012) Palaeozoic multiphase magmatism at Barleik Mountain, southern West Junggar, Northwest China: implications for tectonic evolution of the West Junggar. *International Geology Review* **55**, 633–56.

Yang GX (2012) *Geological characteristics and tectonic evolution of Paleozoic ophiolitic mélange in the West Junggar*. Ph.D. thesis, Chang'an University, Xi'an, China. Published thesis (in Chinese with English abstract).

Yang GX, Li YJ, Tong LL, Li GY, Wu L and Wang ZP (2016) Petrogenesis and tectonic implications of Early Carboniferous alkaline volcanic rocks in Karamay region of West Junggar, Northwest China. *International Geology Review* **58**, 1278–93.

Yang HS, Tian YZ, Yang JS and Tian YL (2019) Geochemistry and geochronology of diabase from Akebastao ophiolitic mélange in western Junggar, Xinjiang, and its tectonic signification. *Acta Geologica Sinica* **93**, 2209–25 (in Chinese with English abstract).

Yang W, Wang GC, Zong RW, Xiao L, Li L and Yang G (2015) Determination of Silurian-Devonian arc-basin pattern in western Junggar and its regional tectonic significance. *Earth Science* **40**, 448–60+503 (in Chinese with English abstract).

Yi SX, Li YJ, Jiao GL, Yang GX, Wang JN and Yang FZ (2014) The establishment and tectonic settings implication of volcanic rocks which belongs to the Early Carboniferous in the Boshchekul-Chingiz volcanic arc, West Junggar. *Xinjiang Geology* **32**, 14–8 (in Chinese with English abstract).

Yin JY, Chen W, Xiao WJ, Yuan C, Windley BF, Yu S and Cai K (2017) Late Silurian-Early Devonian adakitic granodiorite, A-type and I-type granites in NW Junggar, NW China: partial melting of mafic lower crust and implications for slab roll-back. *Gondwana Research* **43**, 55–73.

Yuan HL, Gao S, Liu XM, Li HM, Gunther D and Wu FY (2004) Accurate U-Pb age and trace element determinations of zircon by laser ablation-inductively coupled plasma-mass spectrometry. *Geostandards and Geoanalytical Research* **28**, 353–70. doi: 10.1111/j.1751-908X.2004.tb00755.x.

Zhang C, Santosh M, Liu LF, Luo Q, Zhang X and Liu DD (2018) Early Silurian to Early Carboniferous ridge subduction in NW Junggar: evidence from geochronological, geochemical, and Sr–Nd–Hf isotopic data on alkali granites and adakites. *Lithos* **300–301**, 314–29.

Zhang DY, Zhou TF, Yuan F, White N, Hollings P, Xiao WJ, Deng YF, Zhao BB and Wang JL (2017) Genesis of Late Carboniferous granitoid intrusions in the Dayinsu area, West Junggar, Northwest China: evidence of an arc setting for the western CAOB. *International Geology Review* **59**, 1082–96.

Zhang JE, Xiao WJ, Han CM, Ao SJ, Yuan C, Sun M, Geng HY, Zhao GC, Guo QQ and Ma C (2011) Kinematics and age constraints of deformation in a Late Carboniferous accretionary complex in Western Junggar, NW China. *Gondwana Research* **19**, 958–74.

Zhang L, Wang GC, Gao R, Shen TY, Zong RW and Yan WB (2015) U–Pb chronology of detrital zircons from the Carboniferous sequences and its geological implications in West Junggar. *Geotectonica et Metallogenia* **39**, 704–17 (in Chinese with English abstract).

Zhang P (2020) *Late Paleozoic tectonic transition and evolution of paleo-oceanic basin in Central West Junggar*. Ph.D. thesis, China University of Geosciences, Wuhan, China. Published thesis (in Chinese with English abstract).

Zhang P, Wang GC, Polat A, Zhu CY, Shen TY, Chen Y, Chen C, Guo JS, Wu GL and Liu YT (2018) Emplacement of the ophiolitic mélanges in the west Karamay area: implications for the Late Paleozoic tectonic evolution of West Junggar, northwestern China. *Tectonophysics* **747–748**, 259–80.

Zhang P, Wang GC, Shen TY, Polat A and Zhu CY (2021) Paleozoic convergence processes in the southwestern Central Asian Orogenic Belt: insights from U–Pb dating of detrital zircons from West Junggar, northwestern China. *Geoscience Frontiers* **12**, 531–48.

Zhang YY and Guo ZJ (2010) New constraints on formation ages of ophiolites in Northern Junggar and comparative study on their connection. *Acta Petrologica Sinica* **26**, 422–30 (in Chinese with English abstract).

Zhao K, Chai MR, Zhu R, Zhai JH, Shuang Q and Pan J (2019) Distribution characteristics and genesis of epidote from the Triassic Baikouquan Formation in Xiazijie fan area, Mahu Sag, Junggar Basin. *Journal of Palaeogeography* **21**, 925–38 (in Chinese with English abstract).

Zhao L, He GQ and Zhu YB (2013) Discovery and its tectonic significance of the ophiolite in the south of Xiemisitai Mountain, West Junggar, Xinjiang. *Geological Bulletin of China* **32**, 195–205 (in Chinese with English abstract).

Zhao R, Zhang JY, Zhou CM, Zhang ZJ, Chen S, Stockli DF, Olariu C, Steel R and Wang H (2020) Tectonic evolution of Tianshan-Bogda-Kelameili mountains, clastic wedge basin infill and chronostratigraphic divisions in the source-to-sink systems of Permian-Jurassic, southern Junggar Basin.

Marine and Petroleum Geology **114**, 104200. doi: 10.1016/j.marpetgeo.2019. 104200.

Zheng B, Han BF, Liu B and Wang ZZ (2019) Ediacaran to Paleozoic magmatism in West Junggar Orogenic Belt, NW China, and implications for evolution of Central Asian Orogenic Belt. *Lithos* **338**, 111–27. doi: 10.1016/j. lithos.2019.04.017.

Zheng RG, Zhao L and Yang YQ (2019) Geochronology, geochemistry and tectonic implications of a new ophiolitic melange in the northern West Junggar, NW China. *Gondwana Research* **74**, 237–50.

Zhu YF and Xu X (2006) The discovery of Early Ordovician ophiolite mélange in Taerbahatai Mts., Xinjiang, NW China. *Acta Petrologica Sinica* **12**, 2833–42 (in Chinese with English abstract).

Zong RW, Gong YM and Wang GC (2014) Carboniferous stratal sequence and its palaeogeographical evolution in southern western Junggar, NW China. *Earth Science Frontiers* **21**, 216–33 (in Chinese with English abstract).

Appendix.: LA-ICP-MS U–Pb analytical techniques

Laser sampling was performed using a RESOlution S155-LR 193 nm laser ablation system coupled to an Agilent 7900 ICP-MS. The laser spot size was 40 μm in diameter, the shot frequency was 5 Hz and the energy density was 6 J cm^{-2}. The ablated materials were conveyed into the ICP-MS by a stream of high-purity helium gas with a flux of 280 mL min^{-1}. The sampling method was single-point ablation, and the data acquisition mode was peak jumping (20 ms per isotope for each cycle). The procedure for individual analysis included 10 seconds for the blank, 40 seconds for ablation and 20 seconds for flush. Raw count rates were measured for ^{29}Si, ^{204}Pb, ^{206}Pb, ^{207}Pb, ^{208}Pb, ^{232}Th and ^{238}U. Element concentrations were calibrated by NIST 610 glass and ^{29}Si as the external and internal standards, respectively. Zircon GJ-1 was utilized as the external standard for correction of U–Pb isotope fractionation effects. In addition, Plešovice was used as a secondary standard to monitor the deviation of age. During the analyses, GJ-1 zircon samples were measured twice every eight analyses to correct for instrument drift, Plešovice zircons were measured once every eight analyses to assess the quality of the analyses, and SRM 610 was measured once every eight analyses.

The standard deviation of isotopic ratios and ages of individual analysis points was 1σ, and the weighted average age was 2σ. Analytical details for age and trace and rare earth element determinations of zircons are reported in Yuan *et al*. (2004).

Zircon ages younger than *c.* 1000 Ma are based on ^{206}Pb/^{238}U ratios, and older ages are based on ^{207}Pb/^{206}Pb ratios. The concordance is defined as 100 % × (^{206}Pb–^{238}U age)/(^{207}Pb–^{235}U age) for the former analyses and 100 % × (^{206}Pb–^{238}U age)/(^{207}Pb–^{206}Pb age) for the latter. For the detrital zircons, individual analyses with concordant percentages higher than 90 % were chosen for calculation.